ZnO nanostructures interactions with proteins: *In vitro* fibrillation/antifibrillation studies and *in silico* molecular docking simulations

[1]K. Giannousi, [1]G. Geromichalos, [1]D. Kakolyri, [2,3]S. Mourdikoudis, [1]C. Dendrinou-Samara*

[1]*Laboratory of Inorganic Chemistry, Department of Chemistry, Aristotle University of Thessaloniki, Thessaloniki 54124, Greece*
[2]*UCL Healthcare Biomagnetic and Nanomaterials Laboratories, 21 Albemarle Street, London, W1S 4BS, United Kingdom*
[3]*Biophysics Group, Department of Physics and Astronomy, University College London (UCL), London, United Kingdom*

Abstract

Protein amyloidosis is related to many neurological disorders. Nanoparticles (NPs) due to their small size have the potential to modulate the protein monomers/oligomers assembly into fibril forms, as well as the disaggregation of preformed fibrils. Herein, we have synthesized ZnO nanoflowers and polyol-coated ZnO NPs of relatively small size (40 nm) with cylindrical shape, through solvothermal and microwave-assisted routes. The effect of the different morphology of nanostructures on the fibrillation/antifibrillation process was monitored in bovine serum albumin (BSA) and human insulin (HI) by fluorescence Thioflavin T (ThT) measurements. Although both nanomaterials affected the amyloid formation mechanism as well as their disaggregation, ZnO nanoflowers with their sharp edges exhibited the greatest amyloid degradation rate in both model proteins (73% and 35%, respectively) and inhibited the most the insulin fibril growth, while restrained also the fibrillation process in the case of albumin solution. In order to explain the described *in vitro* activity of ZnO nanostructures, we adopted *in silico* molecular docking studies on the crystal structure of BSA and HI. The binding energy of ZnO NPs was found lower for BSA (-5.44), highlighting their ability to act as catalysts in the fibrillation process of albumin monomers.

Keywords: ZnO, Nanoflowers, Albumin, Insulin, Fibrillation/Antifibrillation, *In silico*

1. Introduction

The interaction of nanoparticles (NPs) with proteins is of major importance in many areas of modern biomedical research, including the emerging fields of nanomedicine and diagnostics.[1] NPs influence the folding state of proteins and affect their aggregation, which is related with the prevention of various disorders related to amyloidosis.[2] The extracellular deposition of a protein in tissues and organs by changing its structure from α-helix to β-leaf (amyloids)[3,4,5] is a common cause and symptom in many neurodegenerative diseases, such as Alzheimer's disease, Parkinson's disease, Huntington's disease (HD), Kreutzfeld-Jacob's

[1]

disease, Prion's disease, and systemic diseases such as amyotrophic lateral sclerosis (Lou Gehrig disease) and type II diabetes. A variety of molecules have been reported in scientific articles as potential inhibitors of amyloid inflammation such as various drugs, small peptides, genes in the context of gene therapy, proteins and chemical osmolyte.[6] The effect of nanoparticles on the formation of protein fibers as well as on the depolymerization of preformed fibers has gained increased interest.[7] Certain types of nanoparticles may accelerate or inhibit the protein fibrillation, but how the size and shape of NPs affect this activity, as well as the related mechanism, remain in infant state.[8]

Among several nanostuctures, metal oxide nanoparticles show promising and far-ranging prospect for biomedical field, especially in what concerns their antibacterial performance, anticancer drug/gene delivery and bio-imaging/sensing.[9] Zinc oxide nanoparticles (ZnO NPs) are among the most widely known types of metal oxide nanoparticles, since they are comparatively cost-effective and mostly safe for bio-applications.[10] Due to their unique physicochemical properties, to the superior antimicrobial and excellent UV blocking properties, they are popularly employed in various fields,[11] such as in the rubber and textile industries,[12,13] in personal care products (cosmetics and sunscreen)[14] as well as in concrete production, photocatalysis and electronics.[15] Thanks to their attractive characteristics, ZnO NPs apart from being already used as food additives, can also take part in metabolism in proteins and nucleic acid synthesis, hematopoiesis, and neurogenesis. In this way, ZnO NPs have received increasing attention in biomedical applications, in particular as anticancer and antibacterial agents, as well as in drug delivery, diabetes treatment, anti-inflammation, wound healing, and bioimaging.[9] However, very few reports are available that showed the inhibition and/or enhancement of amyloid growth by ZnO nanostrcutures, with regard to various amyloid forming proteins and disease models. The inhibitory activity of three different forms of ZnO NPs: uncapped, starch capped and self-assembled was studied on amyloid fibrillation of hen egg white lysozyme and the starch capped NPs exhibited the higher inhibitory effect.[6] Meanwhile, an *in vitro* electrokinetic approach was proposed for evaluating the amyloid degradation ability of ZnO NPs.[16]

In this work, expanding our former research on biomedical applications of metal oxide nanoparticles,[17,18,19,20,21,22,23] we report the wet chemical synthesis of ZnO nanostructures of different morphology, to study their effect on amyloid fibrils formation and degradation in two model proteins; human insulin (HI) and bovine serum albumin (BSA). HI, a blood glucose regulation hormone, can form amyloid fibrils *in vitro* when agitated and/or at acidic pH,[24] while BSA beyond its amyloidogenic property,[25] is a multifunctional protein with extraordinary ligand binding capacity, making it a transporter molecule for a diverse range of metabolites, drugs, nutrients, metals and other molecules.[26] The different morphologies of the ZnO nanostructures was achieved by using solvothermal synthesis with and without the aid of

microwave irradiation and via implementing polyols of different molecular weight. Physicochemical characterization of the as-prepared NPs was conducted with several techniques; X-ray diffraction (XRD), FT-IR and UV/VIS spectroscopies, transmission electron microscopy (TEM) and thermogravimetric analyses (TG). The effect of the ZnO nanostructures of different morphologies in the fibrillation process in terms of amyloid degradation as well as fibril growth delay were monitored by fluorescence Thioflavin T (ThT) measurements and optical fluorescence microscopy. In an attempt to deeper understand the interaction of ZnO NPs with proteins, we proceeded to molecular docking studies on the crystal structure of BSA and HI. Simulations are a useful approach for investigating the binding properties of NPs with key proteins related to amyloid diseases and/or with drug delivery. The *in silico* predictive tools that have been employed to study ZnO NPs interaction with macromolecules, were Spartan ′10, BioMedCaChe and Schrödinger molecular modeling software.

2. Results and discussion

2.1 Synthetic aspects and characterization of ZnO NPs

Amongst metal oxide nanoparticles, zinc oxide nanoparticles have been extensively studied in bio-applications due to their excellent physical and chemical properties, high stability and biocompatibility.[27] It has to be denoted that zinc is an essential trace element and the main component of various enzyme systems while zinc oxide is graded as a "GRAS" (generally recognized as safe) substance by the US Food and Drug Administration (FDA). In the current work, the polyol method has been utilized, which comprises the use of polyalcohols as solvents, reducing agents and surfactants. In that manner, the colloidal stability gets regulated, while control over size, shape, structure and surface chemistry of the resulted nanoparticles (4S characteristics) is assured. Each polyol, in relation to its molecular weight, displays variations regarding its reductive properties and in the ability to form intermediate complexes with the metal precursors.[28] Therefore, the coating mechanism differs, depending also on the chosen reaction parameters (temperature, time, pressure), resulting in NPs of different size and shape.

Herein, two experimental procedures were utilized to synthesize ZnO NPs; solvothermal and microwave-assisted polyol method. Both methods include highly reproducible sealed reaction systems that yield excellent crystalline nanoparticles in a wide range of tuned sizes. These synthetic approaches are green, fast, cheap and simple, although microwave-assisted synthesis is a more energy efficient route that results in the confinement of the reaction time.[29] Upon appropriate synthetic parameters adjustment and by adding either a low molecular weight polyol (diethylene glycol – DEG) or polyethylene glycol of high molecular weight (PEG 8000), ZnO nanostructures of high colloidal stability and different

characteristics were isolated. DEG has been used in the microwave synthesis, whereas PEG in the solvothermal.

Fig. 1a illustrates the x-ray diffractograms of the as-produced ZnO NPs. The observed peaks confirm the formation of hexagonal ZnO NPs (#89-0510) and correspond to reflections from the (1 0 0), (0 0 2), (1 0 1), (1 0 2), (1 1 0), (1 0 3) and (1 1 2) planes, respectively. The appearance of sharp peaks indicates the good crystallinity of the produced ZnO NPs. Based on the intense peak (1 0 1) and on the Scherrer equation the average crystallite sizes for the NPs prepared in the presence of DEG and PEG 8000 were calculated at 16.8 and 26.3 nm, respectively, revealing that the change between the polyols and/or the synthetic methods affects the size.
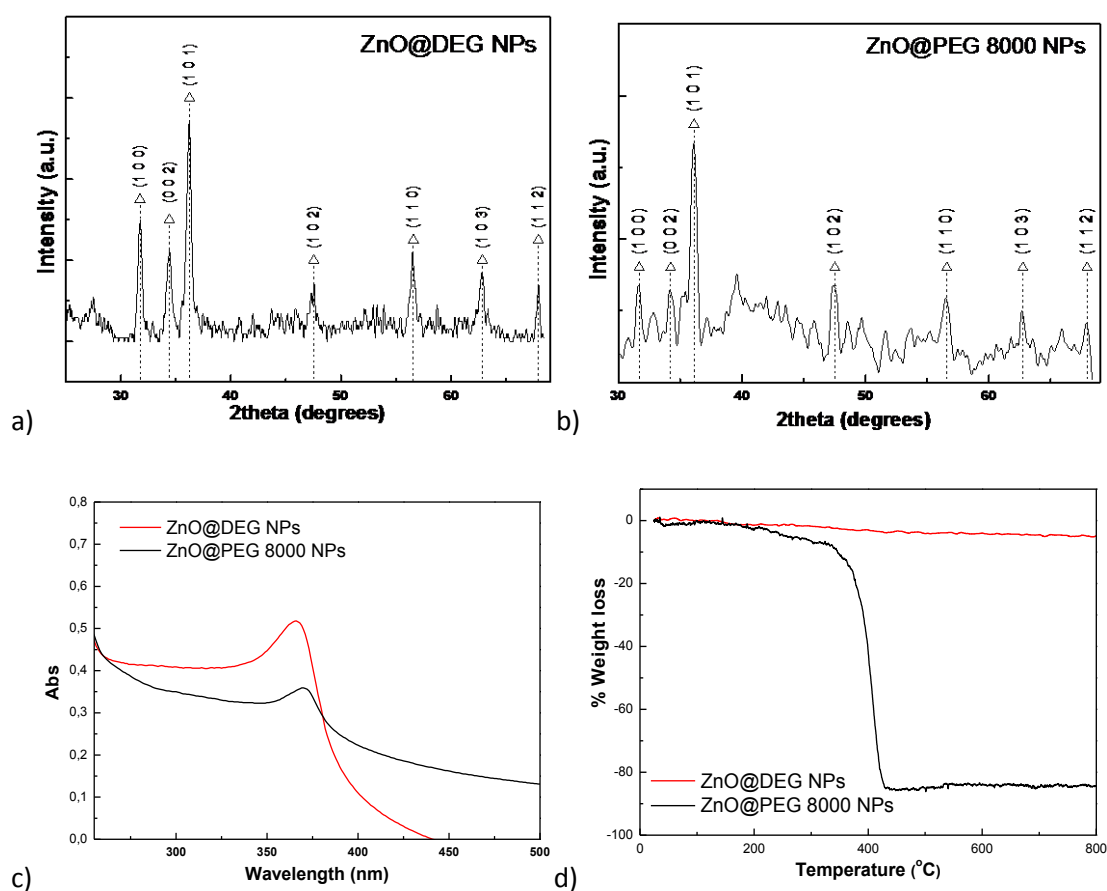

Fig. 1. X-ray diffractograms (XRD) of (a) ZnO@DEG NPs, (b) ZnO@PEG 8000 NPs, UV-VIS spectra (c) and thermogravimetric analysis curves (TGA) of ZnO@DEG (red line) and ZnO@PEG 8000 NPs (black line) (d).

The presence of polyols was certified by FT-IR spectroscopy (**Fig. S1, SI**) and thermogravimetric analysis (TGA) (**Fig. 1d**). NPs prepared in the presence of DEG under microwave irradiation were found with 4.5% w/w organic coating, while the cumulative organic content for ZnO@PEG 8000 NPs lost reaches at 85%. In both cases, the decomposition of the surfactants begins at around 430 °C. The big difference between the

[4]

percentages of organic coatings may be attributed to the molecular weight of the polyol implemented, since it has been previously shown that in the presence of the bulky PEG 8000 a bigger amount of surfactant binds onto the surface of the NPs.[30, 31] The composition was further verified by UV-VIS spectroscopy (**Fig. 1c**), where ZnO nanoparticles are expected to show a peak at 350-390 nm.[32] ZnO@DEG NPs appear peak at 367 nm, whereas ZnO@PEG 8000 NPs at 370 nm. The slight redshift in the last case may be attributed to the smaller band gap and the marginally bigger size of the NPs.

Morphological particle characteristics of ZnO NPs were investigated with electron microscopy. TEM images of the NPs are shown in **Fig. 2**. The ZnO NPs prepared in the presence of DEG in the triple role of solvent, surfactant and reducing agent appeared to possess a nanoflower structure. Similar Pt nanoflowers have been reported previously via reduction of Pt acetylacetonate (Pt(acac)$_2$) with analogous wet chemical synthesis, by using DEG as a solvent and polyethylenimine (PEI) as a capping agent.[33] In the above study, it was emphasized the important role of DEG in the formation of the nanoflowers. Jørg. J. Schneider *et al.* in 2010 reported ZnO NPs grouped in agglomerates with blackberry structure.[34] However, in our case the nanostructures with the sharp edges and the high surface area (**Fig. 2a, b**) seem to be developed through oriented aggregation and thus are denoted as nanoflowers of 168 ± 14 nm, as calculated from the histogram chart (**Fig. 2a inset**). In case of ZnO@PEG NPs the nanoparticles appeared well dispersed, having a cylindrical shape and their size is approximately 40 ± 1.4 nm (**Fig. 2c, d**).
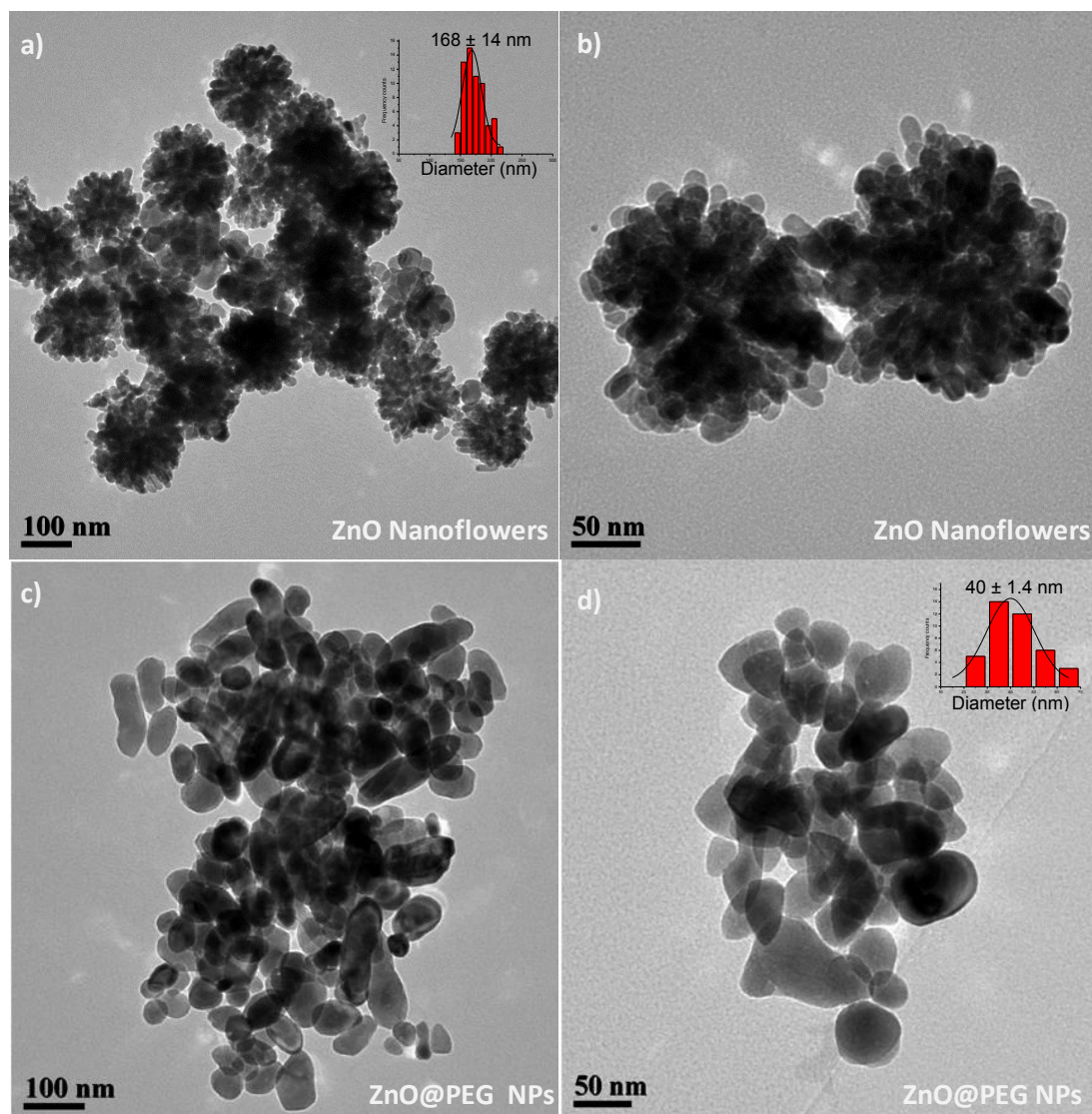
Fig. 2. TEM images of ZnO Nanoflowers (a and b) and ZnO@PEG NPs (c and d). Frequency counts of over 100 particles, size and standard deviation of nanoflowers 168 ± 14 nm and of ZnO@PEG NPs 40 ± 1.4 nm (Insets).

### 2.2 Fibrillation/Antifibrillation Studies by ZnO NPs

Thioflavin-T (ThT) fluorescence assay was used to confirm the presence of amyloids due to the selective binding with amyloid fibrils. The transformation of the native forms of proteins into amyloid fibrils, characterized by high cross β-sheet contents, is associated with significant increase of ThT emission intensity.[35] The total kinetics of protein and peptide aggregation follows three phases and begins with monomeric peptide or protein units. The first phase (lag phase, phase 1) involves the formation of nuclei until they obtain a critical core size (nucleation) to initiate an exponential phase of fiber growth (elongation phase-growth regime, phase 2) with the sigmoidal pattern characteristic of kinetic aggregation of the amyloidogenic peptides into insoluble fibrils. The third phase is a static phase (plateau regime).[7] Acetylsalicylic acid (ASA) was also included in our studies as a positive control,

since it induces transition from α-helix to β-sheet and increased propensity for protein aggregation.[36] The fluorescence spectra are expressed as % protein fibrillation, with the fluorescence signal corresponding to 100% fibrillation status in case of agitation of the maximum concentration of neat protein.

Initially, we analyzed the effect of different concentrations of NPs (5-35 μg/mL) on the fibrillation process of insulin and albumin after agitation and incubation for 20 min at 37 °C. Although the insulin polymerization increases with the NPs concentration, it still remains constrained compared to the process without NPs. The NPs were added at the control lag phase, since it has been reported that once critical nuclei are formed, the elongation process is so favorable that the addition of NPs does not have any effect on oligomer interactions with nanoparticles.[7] The diagrams illustrated in **Fig. 3 a and b** show the % fluorescence intensity for the maximum concentration of acetylsalicylic acid (ASA), ZnO and ZnO@PEG NPs (35 μg/mL) on the maximum concentration of insulin and BSA (250 μg/mL), respectively. ASA causes an increase in the fluorescence signal of both proteins with the respective intensities reaching 123% and 206%. Acetylation with ASA enhances the process of fibrillation, since this type of modification has significant structural destabilizing effect which finally makes the protein more vulnerable for pathogenic aggregation.[36] The more pronounced effect in case of albumin may reflect the different structural characteristics of albumin.[37] The same tendency was preserved in the presence of the nanoparticles for albumin; ZnO nanoflowers caused a slight increase in the intensity (106%), whereas ZnO@PEG NPs provoked a rather significant increase (177%). The variations in the activity of the NPs can be attributed to the morphology differences. The sharp edges and larger surface area of nanoflowers (168 nm) seem to restrain the balance between fibrillation and antifibrillation resulting in a spectrum similar to the neat protein solution when compared to the cylindrical nanoparticles of 40 nm.

On the contrary, both types of nanoparticles cause a reduction in the insulin fibril formation. The largest decrease is caused by ZnO nanoflowers with a rate of about 47%, followed by the ZnO@PEG NPs with a rate of 44%. The monodispersity and the tuned surface characteristics of the as-prepared ZnO nanostructures seem to affect the inhibition of amyloid formation, as starch-capped ZnO NPs of 30 nm were found to inhibit amyloid formation in a similar extent,[6] whereas uncapped ZnO NPs of 10 nm affected less the fibrillation process.[6] Meanwhile, bare spherical polydispersed ZnO NPs (20-30 nm) enhanced insulin fibrillation.[38] The opposite behaviors of the as-prepared NPs observed in the two protein solutions (albumin and insulin) are mainly attributed to the differences in the amino acid sequences within and on the surface of the insulin and albumin amyloid fibrils, which in turn result in different intrinsic stabilities and opportunities for affecting the hydrogen bonds forming the β-sheets of fibrils.[39] Based on previous studies, BSA is more prone on forming oligomeric forms,[40,41] and the NPs appear to boost its fibrillation process with specificity.

[7]

Concerning human insulin, it is stored in the B-cells of pancreas as a 2Zn-coordinated inactive hexamer.[42] Monomeric and dimeric forms of insulin (the physiologically active forms) are less stable than hexamer and are prone to form amyloid fibrillar aggregates.[43] In that manner, zinc ions leaching from the NPs can stabilize insulin hexamers and thus the fibrils cannot be regenerated.
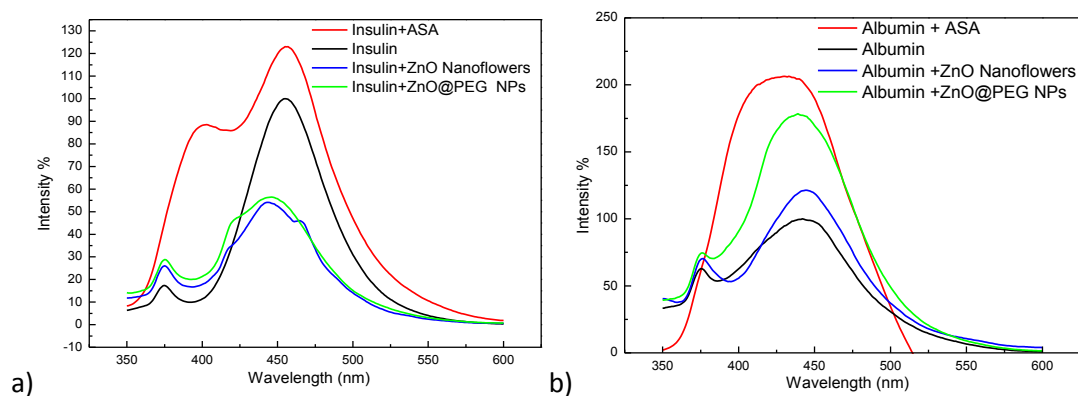
Fig. 3. ThT fluorescence assay of 250 μg/mL human insulin (a) and bovine serum albumin (b) amyloid fibrils expressed as % intensity. ZnO and ZnO@PEG NPs of 35 μg/mL were added, and the spectra were recorded. Each curve represents the mean values of three independent experiments. Acetylsalicylic acid (ASA) (35 μg/mL) was also included in the assay as a positive control for the fibrillation status.

We studied further the ability of ZnO NPs to degrade amyloids. Mature fibrils were formed by proper agitation and incubation of protein solutions at 37 $^{\circ}$C for 20 min, while the presence of amyloids was confirmed using ThT fluorescence assay. The antifibrillation process was found concentration-dependent, in agreement with a previous study with glycine coated Fe_3O_4 MNPs (Gly-MNPs),[35] with the effect being more pronounced in case of insulin. Antosova *et al.* have recently reported the ability of the Gly-MNPs to degrade insulin fibers but the concentration needed to destroy 50% of amyloid fibrils was high (130.9 μg/mL) compared to the values tested in this study.[35] The fluorescence spectra expressed as % protein fibrillation are presented in **Fig. 4.** The injection of 35 μg/mL nanoparticles in the insulin solution led to almost total breakdown of the fibrils' net with decline in the fluorescence intensities of about 73% and 67% for ZnO nanoflowers and ZnO@PEG NPs, respectively (**Fig. 4a**). The degradation effect in case of albumin net remained countable but significantly attenuated; the respective intensity rates were approximately 65% and 82% (**Fig. 4b**). The ZnO nanoflowers constitute a better candidate for amyloid degradation compared to ZnO nanoparticles due to higher surface to volume ratio and to the sharp edges of the petals in agreement with previous study.[16] Girigoswami *et al.* have also shown that nanoflowers have significantly higher amyloid destroying capacity compared to spherical ZnO NPs but the degradation rate of insulin amyloids never exceeded 65%.[16]

[8]
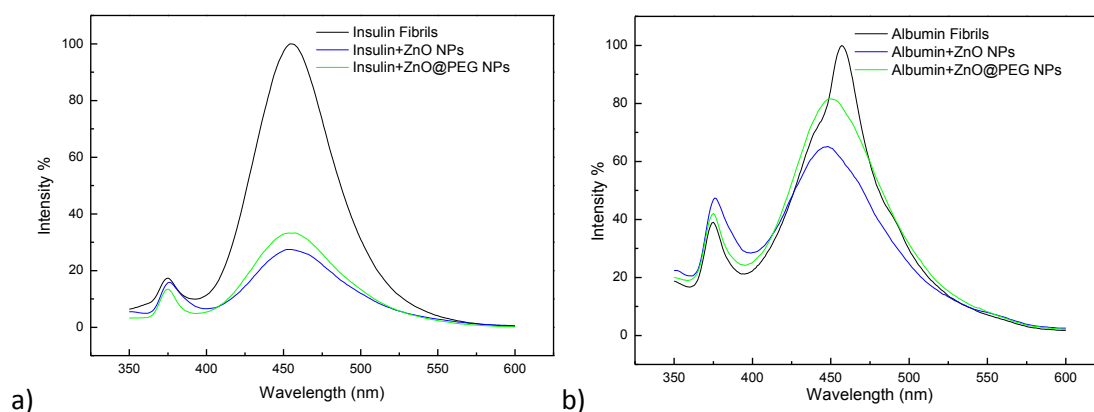
Fig. 4. ThT fluorescence assay of 250 μg/mL human insulin (a) and bovine serum albumin (b) amyloid fibrils expressed as % intensity. ZnO and ZnO@PEG NPs of 35 μg/mL were added in the mature fibrils, and the spectra were recorded. Each curve represents the mean values of three independent experiments.

2.3 Docking calculations

The calculated global binding energies of ZnO NPs docked on BSA and HI targets, are -5.44 and -1.56, respectively, highlighting the ability of ZnO NPs to succeed better binding (lower binding energy) for BSA than with HI. These data may in part explain the observed *in vitro* activities of ZnO NPs. The crystal structure of BSA with depiction of the most probable ligand binding sites and also the designation of sub-domains and helices, are shown in **Fig. 5**. The secondary structure of BSA shown with the subdomains color-coded is assigned based on Majorek *et al.*[44]
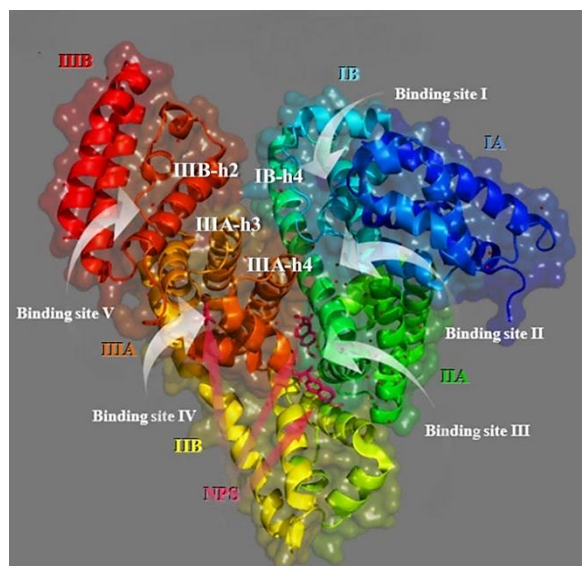

Fig. 5. Drug-binding sites of BSA (PDB ID 4OR0) identified by the literature. Target protein is illustrated as cartoon with sub-domains color-coded according to chainbow with additional depiction of semi-transparent surface colored also by chainbow. Co-crystallized drug naproxen (NPS) (depicted in stick model and colored according to atom type in hot pink C atoms) is also illustrated. In the crystal structure of the protein is depicted the binding sites I,

II, III, IV and V, belonging to labeled proteins' sub-domains, IA, IIA, IIIA, IB, IIB and IIIB. The final structure was ray-traced and illustrated with the aid of PyMol Molecular Graphics System.

The computational approach revealed that ZnO nanoparticle is anchored in a cavity of BSA protein formed by domains IB, IIA, IIIA and IIIB (**Fig. 6**). The binding pocket is formed by helices IB-h4, IIIB-h2, IIIA-h3 and IIIA-h4, between binding sites I, II, IV and V (illustrated in **Fig. 5**). Zn and O atoms of ZnO NP are making hydrogen-bond (H-b) and polar (P) contacts with the amino acid residues of BSA and HI target proteins' binding sites. Binding interactions for both macromolecule target proteins, are illustrated in Table S1 (in the SI). Since the docked molecule ZnO NP is positioned in an allosteric binding site, different from the three binding sites occupied by NPs, no common binding contact is found between the two ligands. The binding architecture of ZnO NP docked into HI protein is depicted in **Fig. 7**.
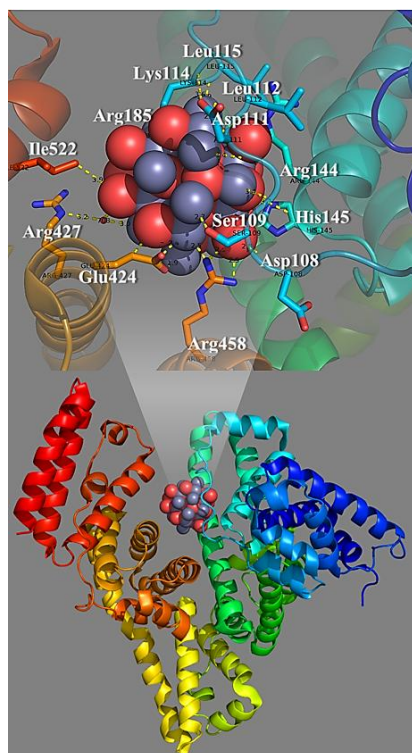

Fig. 6. Docking pose of ZnO NP into BSA (PDB entry code 4OR0) (chain A). The best pose for ZnO NP is positioned in a crevice of the protein formed by helices IB-h4, IIIB-h2, IIIA-h3 and IIIA-h4, between binding sites I, II, IV and V. ZnO NP is illustrated in sphere representation and colored according to atom type: red for O atoms and grey for Zn atoms. Target protein is illustrated as cartoon with sub-domains color-coded according to chainbow. A close-up view of the binding cavity is shown in the upper part of the figure with depth cue in the raytracing rendering of the cartoon. Selected contacting amino acid residues of the binding pocket are rendered in stick model and colored according to atom type (N and O atoms, blue and red, respectively) and helices (C atoms according to chainbow). Binding contacts are shown as yellow dotted lines. H atoms are omitted for clarity. The final structure was ray-traced and illustrated with the aid of PyMol Molecular Graphics System.
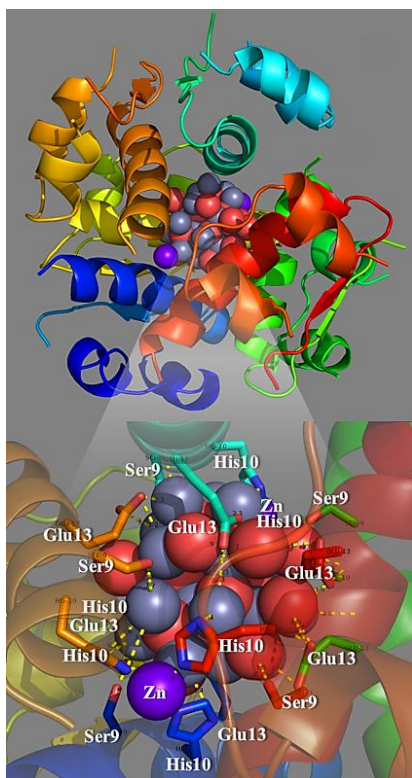
Fig. 7. Molecular docking of ZnO NPs into hexameric structure of HI (PDB ID 6GNQ). The co-crystallized CRS is deleted and only the six chain-stabilizing Zn^{2+} ions are illustrated. Target protein is illustrated as cartoon with the six chains color-coded according to chainbow. ZnO NP is anchored in the center of the protein, in a cavity formed between the six symmetry- related chains. ZnO NP is illustrated in sphere representation and colored according to atom type: red for O atoms and grey for Zn atoms. The two Zn ions co-crystallized in the hexameric structure are depicted in sphere representation in magenta color. A close-up view of the binding cavity is shown in the lower part of the figure with depth cue in the raytracing rendering of the cartoon. Selected contacting amino acid residues of the binding pocket are rendered in stick model and colored according to atom type (N and O atoms, blue and red, respectively) and helices (C atoms according to chainbow). Binding contacts are shown as yellow dotted lines. H atoms are omitted for clarity. The final structure was ray-traced and illustrated with the aid of PyMol Molecular Graphics System.

From docking pose it is deduced that ZnO NP is positioned in the center of the protein, between the two Zn^{2+} ions in the hexameric HI protein which stabilize the proteins' structure. It is obvious that the pocket has the ability to accommodate both Zn ions and ZnO nanostructures at the same place. The amino acid resides contributing in the stabilization of ZnO NP in the binding cavity of HI protein are revealed to be Ser9, His10 and Glu13. His10 residues seems to play a critical role on the binding of the docked molecule, as is also shown by Karavassili *et al*.[45] His10 and Glu13 residues are also identified as critical in the binding by a molecular dynamic (MD) simulation of ZnO NP on insulin target protein.[46] ZnO NP binding architecture shows that the nanostructure occupies the same place as the Zn^{2+} ions in the native HI protein (PDB ID: 6GNQ). The hexameric structure of HI protein contains six

chains and is stabilized with two Zn ions connected with three symmetry- related histidine molecules (His10). Zn^{2+} ions are connected with polar contact with NE2 of His10 in 1st, 2nd and 3rd chain (2.0, 1.9 and 2.0 Å, respectively) of the native HI protein (**Fig. 8a**) colored according to atom type (N and O atoms, blue and red, respectively) and helices (C atoms orange, red and blue, respectively). Similarly, in **Fig. 8b** is illustrated the binding of protein's native Zn^{2+} ion with NE2 of His10 in 4th, 5th and 6th chain (2.0, 2.0 and 1.9 Å, respectively) of the native HI protein colored according to atom type (N and O atoms, blue and red, respectively) and helices (C atoms teal, green and yellow, respectively).
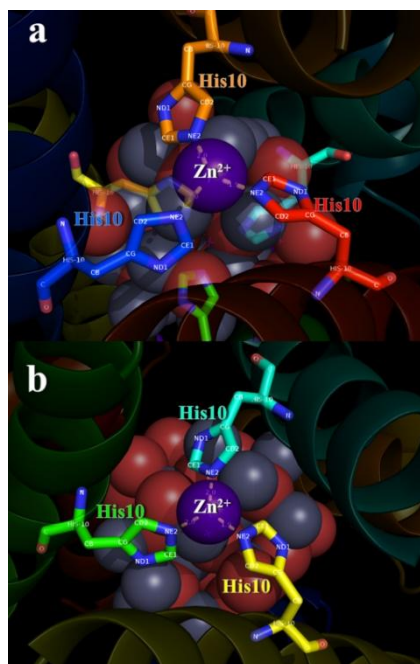
Fig. 8. Binding architecture of Zn^{2+} ions in the native HI protein (PDB ID: 6GNQ) superimposed with the binding pose of ZnO nanoparticle. The hexameric structure of HI protein contains six chains and is stabilized with two Zn ions connected with three symmetry- related histidine molecules (His10). Zn^{2+} ions (represented as spheres in magenta color) are connected with polar contact with NE2 of His10 in 1st, 2nd, 3rd (a) and 4th, 5th and 6th (b) chains. Target protein is illustrated as cartoon with the six chains color-coded according to chainbow. ZnO NP is illustrated in sphere representation and colored according to atom type: red for O atoms and grey for Zn atoms. Amino acid residues are render in stick mode and colored according to atom type (N and O atoms, blue and red, respectively) and helices for C atoms: orange, red and blue (a) for 1st, 2nd and 3rd chains, respectively, and teal, green and yellow for 4th, 5th and 6th chains, respectively.

Overall, the results indicate that ZnO nanostructures bind more easily with BSA monomers than with insulin ones; they act as catalysts and facilitate the assembly of oligomers into stable fibril aggregates boosting that manner the fibrillation process.[7] However, the NPs cannot interfere with the same ability in the BSA mature fibrils' net and the degradation rate remains low as opposed with insulin net, where the NPs are more efficient in destroying the amyloids. Hence, the nature of the studied protein as well as the

morphology of the NPs proved to be the key factors affecting the interaction of the nanostructures with monomers/oligomers and amyloids. Furthermore, our findings support that ZnO nanoflowers can be used as a potent anti-amyloid agent and become a possible drug candidate for amyloidosis.

3. Materials and Methods

Materials: All the reagents were of analytical grade and were used without any further purification. The products necessary for our experiments are the following: Zinc acetylacetonate hydrate $C_{10}H_{14}O_4Zn \cdot xH_2O$ (Aldrich, M=263.61 g/mol), Zinc nitrate tetrahydrate $Zn(NO_3)_2 \cdot 4H_2O$ (Merck, M= 261.44 g/mol), polyethylene glycol (PEG) 8000 (Alfa aesar), diethylene glycol (DEG) (Aldrich), Thioflavin T (J&K Scientific GmbH, 98%), Human insulin (Actrapid), Bovine serum albumin (J&K Scientific GmbH, 98%), PBS Dulbecco's Phosphare Buffered Saline (biowest).

Preparation of ZnO NPs: For ZnO@PEG 8000 NPs the polyol process under solvothermal conditions was used. 0.28 g $Zn(acac)_2$ and 1 g PEG 8000 were mixed and dissolved. The solution was stirred thoroughly and then transferred into a Teflon-lined stainless-steel autoclave. The process was carried out under autogenous pressure at 200 °C for 8 h. Then the liquids were centrifuged at 5000 rpm for 20 min and a black-brown and light brown precipitate respectively, was obtained and washed with ethanol (5000 rpm, 20 min), at least three times, to remove the unreacted precursors. For ZnO@DEG NPs the polyol process under microwave conditions was used. 0.561 g $Zn(acac)_2$ were dissolved in 40 mL DEG. The solution was stirred thoroughly and then transferred into a Teflon. The process was carried out in a microwave oven under pressure at 260 °C for 30 min. Then the liquid was cooled, centrifuged at 5000 rpm and a white precipitate was obtained and washed with ethanol, at least three times, to remove the unreacted precursors.

Characterization: X-ray powder diffraction (XRD) measurements were performed on a Philips PW 1820 diffractometer at a scanning rate of 0.050/3 s, in the 2θ range from 10 to 90°, with monochromatized Cu-K$_\alpha$ radiation (λ= 1.5406 nm). Conventional Transmission Electron Microscopy (TEM) images were obtained with JEOL100 CX microscope operating at 100 kV. For TEM observations we have used suspensions of the nanoparticles deposited onto carbon-coated copper grids. Fourier transform infrared spectra (FTIR) (450–4000 cm^{-1}) were recorded using a Nicolet FT-IR 6700 spectrometer with samples prepared as KBr pellets. Thermogravimetric analysis (TGA) was performed using SETA-RAM SetSys-1200 and carried out in the range from room temperature to 800 °C at a heating rate of 10 °C min^{-1} under N_2 atmosphere. Powder X-ray diffraction (XRD) was performed using a 2-cycle Rigaku

Ultim$_{a+}$ diffractometer (40 kV, 30 mA, Cu-K$_\alpha$ radiation) with Bragg–Brentano geometry (detection limit 2 % approximately). Fluorescence spectra were recorded in solution on a Hitachi F-7000 fluorescence spectrophotometer.

Sample preparation and Thioflavin (THT) assay: A ThT stock solution was prepared by adding 10 mg Thioflavin to 10 mL PBS. The fluorescence intensity of the solutions was measured by excitation at 330 nm with a slit width of 5 nm. First, the polymerization of the two proteins and the interaction with ZnO NPs and ASA was studied with concentration and time. A solution containing 10 μL of protein (15 μg/mL), 2 mL of PBS and 10 μL of ThT was measured by excitation at 330 nm. The measurements were repeated by adding 10 μL of insulin until concentration reaches 250 μg/mL and then the protein fibrillation was studied in time (per 5 minutes). Solutions which contained 10 μL of protein (15 μg/mL), 2 mL of PBS with/without 5 μg/mL of NPs or ASA were incubated at 37 ^{o}C for 20 min, and then 10 μL of ThT were added to measure the fluorescence signal according to the above procedure. The measurements were repeated by adding 10 μL of NPs or ASA until the concentration reached 35 μg/mL and the protein fibrillation was studied in time per 5 minutes. Moreover, the depolymerization of the two proteins was studied. The protein fibrils were formed by agitating and incubating the protein solution, which contained 200 μL of protein (250 μg/mL) and 2 mL of PBS, at 37 ^{o}C for 20 min. Afterwards, 70 μL of NPs and 10 μL of ThT were added and the signal was measured upon excitation at 330 nm. The measurements were recorded every 1 minute until reaching a steady state.

In silico computational methods (molecular modeling and docking calculations)

The *in silico* predictive tools that have been employed to study the ZnO NP to interact with macromolecules, are Spartan ′10, BioMedCaChe and Schrödinger molecular modeling software. Molecular model of ZnO NP with Zn and O atoms arranged in a hexagonal wurtzite-type crystal structure was built in 3D coordinates and its best, most stable (lowest energy) conformation was detected by geometrical optimization in the gas phase, as implemented in the Spartan'14 Molecular Modeling program suite (Spartan '08 v.1.1.4, Wavefunction Inc., Irvine, CA, USA; www.wavefun.com). The structure was initially optimized (via energy minimization) by conformational search using the Monte Carlo method with the MMFF94 molecular mechanics model, included in the Spartan'14 program suite. Geometry optimization (leading to the most stable conformer with the lowest energy) was accomplished via quantum-chemical calculations by utilizing the ab initio Hartree-Fock method with a 6-31G* basis set.

Molecular docking

The molecular docking studies were carried out on the crystal structure of BSA and HI target proteins to investigate the effect of ZnO NP on these proteins. All crystal structures of

the studied proteins were obtained from the Brookhaven Protein Data Bank (operated by the Research Collaboratory for Structural Bioinformatics, RCSB).[47] The chosen X-ray structure of BSA protein is in complex with bound co-crystallized drug naproxen (NPS, (S)-2-(6-methoxynaphthalen-2-yl)propanoic acid) (refined at 2.58 Å resolution),[48] while the monoclinic crystalline form of HI is conjugated with meta-cresol (CRS) (refined at 2.20 Å resolution) (released: 2019-06-12). Protein Data Bank, PDB entry codes for BSA and HI are 4OR0 and 6GNQ, respectively.

For the docking calculations, only the A chain of the BSA protein was used, since chain B is replicate, with NPS bound at the same ligand binding site among the chains. The 6GNQ PDB file of HI protein contains two hexameric structures with six chains each, co-crystallized with m-cresol and stabilized with four Zn^{2+} ions, two for each hexameric structure. For the docking of ZnO NP in HI, only one hexameric structure was used, since the two structures are identical. For this reason, the data for chain B of BSA and the six chains of the second hexameric structure of HI, as long as each ligand and metal ion referring to these chains, were deleted from corresponding PDB files.

The molecular docking simulation was performed in project leader of BioMedCAChe 7.5 computer-aided chemistry software package, which is part of the CAChe package (CAChe WorkSystem Pro version 7.5.0.85, Fujitsu Co. Ltd., Tokyo, Japan). BioMed CaChe engages a stochastic optimization method to enhance the intra-molecular energy of a ligand by rotation and analyzing various orientations. BioMed CAChe automates the docking of ligand into active or binding sites by using a genetic algorithm with a fast, simplified potential mean force (PMF). The potential of mean force is a knowledge-based approach that extracts pairwise atomic potentials from structure information of known protein-ligand complexes contained in the PDB.

Docking was carried out at full rotation allowing full flexibility for the ligand while keeping the target protein fixed in space. Docking parameters involved steric scan, final search for ligand binding site and refinement of the complex. Cache docking score performs force fields which includes terms as bond stretching, angle bending, torsional, and nonbonded interactions such as Vander Waals and Hydrogen bond interactions. The molecule-based scoring function and is made up of four components: 1. Protein-ligand H-bond energy (external H-bond). 2. Protein-ligand van der Waals energy (external vdw). 3. Ligand internal van der Waals energy (internal vdw). 4. Ligand intramolecular H-bond energy (internal H-bond). Docking Score = S (hb_ext) + S (vdw_ext) + S (hb_int) + S (vdw_int). The produced compound-protein conjugates were ranked by the energy score, including their binding conformations. Best docked poses, with both lower binding energies and stronger interaction pattern, were derived from a number of solutions (docking results), usually with the higher ranking.

Three-dimensional (3D) models of BSA and HI crystal structures were developed, after the deletion of the co-crystallized bound ligands. The final output of the docking procedure is a set of solutions (docking results) ranked according to the corresponding scoring function values, each defined by the 3D coordinates of its atoms and expressed as a PDB file. In this study, the docking procedure with the aid of BioMedCAChe was shown to accurately reproduce experimentally observed binding modes of NPS and CRS, in terms of RMSD (root-mean squared deviation). The BioMedCAChe provided excellent results as low values of RMSD (best docked solutions of docking results 0.29 Å and 0.25 Å, respectively) were observed between the experimental and the best-scoring docked structures derived by superimposition of these structures (the accuracy of the docking results are good when the RMSD is mostly below 1.0 Å). The ability to accurately predict the binding conformation of the ligands and substrates, gave confidence that the BioMedCAChe would also exhibit a similar accuracy with the investigated ZnO NP in the study. The PyMol Molecular Graphics System (Schrödinger, LLC. version 1.8.2.0, www.pymol.org), was used to visualize the molecules and analyze the results of the docking and to construct the molecular models.[49]

Supporting Information

Additional data with FT-IR measurements of the ZnO NPs and binding interactions of ZnO NPs with BSA and HI (Atom numbering and bond lengths are derived from PyMol software). This material is available free of charge via the Internet.

Conflict of interest

The authors declare that there are no conflicts of interest.

Author Contributions

Author Contributions: Conceptualization, C.D-S. and K.G.; methodology, C.D-S., D.K. and K.G.; validation, K.G.; formal analysis, K.G.; TEM images S.M.; simulation data G.G.; investigation, K.G.; resources, C.D-S., G.G., and K.G.; data curation, G.G., S.M. and K.G.; writing—original draft preparation, K.G. and G.G.; writing—review and editing, C.D-S. and S.M.; visualization, K.G.; supervision, C.D-S.; project administration, C.D-S.

4. References

[1] M. Kopp, S. Kollenda, and M. Epple, Nanoparticle−Protein Interactions: Therapeutic Approaches and Supramolecular Chemistry, *Acc. Chem. Res.* 2017, 50, 1383−1390.

[2] R. Parveen, T.N. Shamsi, S. Fatima, Nanoparticles-Protein Interaction: Role in Protein Aggregation and Clinical Implications, *International Journal of Biological Macromolecules* 2016, S0141-8130(16)31070-4, DOI: http://dx.doi.org/doi:10.1016/j.ijbiomac.2016.10.024.

[3] M.F. Khan, R.H. Falk, Amyloidosis, *Postgrad Med J* 2001, Vol. 77, Pages: 686–693.

[4] R.S. Harrison, P.C. Sharpe, Y. Singh, D.P. Fairlie, Amyloid peptides and proteins in review, *Rev Physiol Biochem Pharmacol* 2007, Vol. 159, Pages:1 –77.

[5] A. Prasansuklab and T. Tencomnao, Amyloidosis in Alzheimer's Disease: The Toxicity of Amyloid Beta (Aβ), Mechanisms of Its Accumulation and Implications of Medicinal Plants for Therapy, *Evid Based Complement Alternat Med.* 2013, Pages: 413808.

[6] Deependra Kumar Ban and Subhankar Paul, Nano Zinc Oxide Inhibits Fibrillar Growth and Suppresses Cellular Toxicity of Lysozyme Amyloid, *ACS Appl. Mater. Interfaces* 2016, Vol. 8, Pages: 31587−31601.

[7] M. Zaman, E. Ahmad, A. Qadeer, G. Rabbani, R. Khan, Nanoparticles in relation to peptide and protein aggregation, *Int J Nanomedicine* 2014, Vol. 9, Pages: 899–912.

[8] T. John, A. Gladytz, C. Kubeil, L.L. Martin, H.J. Risseladaa, and Bernd Abel, Impact of nanoparticles on amyloid peptide and protein aggregation: a review with a focus on gold nanoparticles, *Nanoscale* 2018, Volume:10, Issue: 45, Pages: 20894-20913.

[9] Jinhuan Jiang, Jiang Pi, and Jiye Cai, The Advancing of Zinc Oxide Nanoparticles for Biomedical Applications, *Hindawi Bioinorganic Chemistry and Applications* 2018, Vol. 3, Pages: 18.

[10] P.K. Mishra, H. Mishra, A. Ekielski, S. Talegaonkar, and B. Vaidya, Zinc oxide nanoparticles: a promising nanomaterial for biomedical applications, *Drug Discovery Today* 2017, vol. 22, no. 12, pp. 1825–1834.

[11] A. Kolodziejczak-Radzimska and T. Jesionowski, Zinc oxide–from synthesis to application: a review, *Materials* 2014, vol. 7, no. 4, pp. 2833–2881.

[12] S. Sahoo, M. Maiti, A. Ganguly, J. J. George, and A. K. Bhowmick, Effect of zinc oxide nanoparticles as cure activator on the properties of natural rubber and nitrile rubber, *Journal of Applied Polymer Science* 2007, vol. 105, no. 4, pp. 2407–2415.

[13] A. Hatamie, A. Khan, M. Golabi et al., Zinc oxide nanostructure-modified textile and its application to biosensing, photocatalysis, and as antibacterial material, *Langmuir* 2015, vol. 31, no. 39, pp. 10913–10921.

[14] M. D. Newman, M. Stotland, and J. I. Ellis, The safety of nanosized particles in titanium dioxide- and zinc oxide based sunscreens, *Journal of the American Academy of Dermatology* 2009, vol. 61, no. 4, pp. 685–692.

[15] F.X. Xiao, S.F. Hung, H.B. Tao, J. Miao, H.B. Yang, and B. Liu, Spatially branched hierarchical ZnO nanorod-TiO$_2$ nanotube array heterostructures for versatile photocatalytic and photoelectrocatalytic applications: towards intimate integration of 1D-1D hybrid nanostructures, *Nanoscale* 2014, vol. 6, no. 24, pp. 14950–14961.

[16] Agnishwar Girigoswami, M. Ramalakshmi, Najim Akhtar, Sanjay Kisan Metkar, Koyeli Girigoswami, ZnO Nanoflower petals mediated amyloid degradation - An in vitro electrokinetic potential approach, *Materials Science and Engineering: C* 2019, Volume 101, Pages: 169-178.

[17] K. Giannousi, O. Antonoglou, C. Dendrinou-Samara, Interplay between Amyloid Fibrillation Delay and Degradation by Magnetic Zinc-Doped Ferrite Nanoparticles, *ACS Chem Neurosci.* 2019, 10(8):3796-3804.

[18] E. Christodoulou, M. Nerantzaki, S. Nanaki *et al.* Paclitaxel magnetic core–shell nanoparticles based on poly(Lactic acid) semitelechelic novel block copolymers for combined hyperthermia and chemotherapy treatment of cancer, *Pharmaceutics* 2019, 11 (5), Article number 213.

[19] K. Giannousi, E. Koutroumpis, V. Georgiadou, V. Karagkounis, C. Dendrinou-Samara, Nanoplatforms of manganese ferrite nanoparticles functionalized with anti-inflammatory drugs, *Eur. J. Inorg. Chem.* **2019**, 14, 1895-1903.
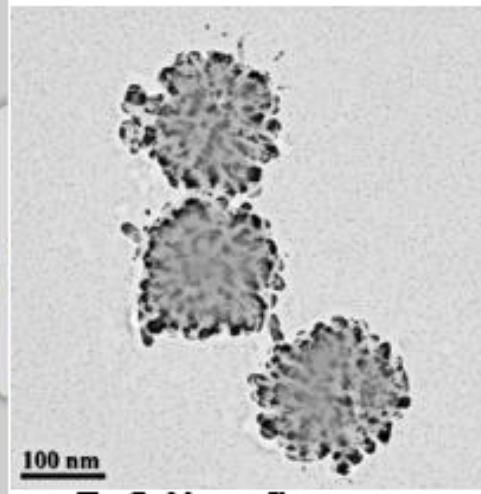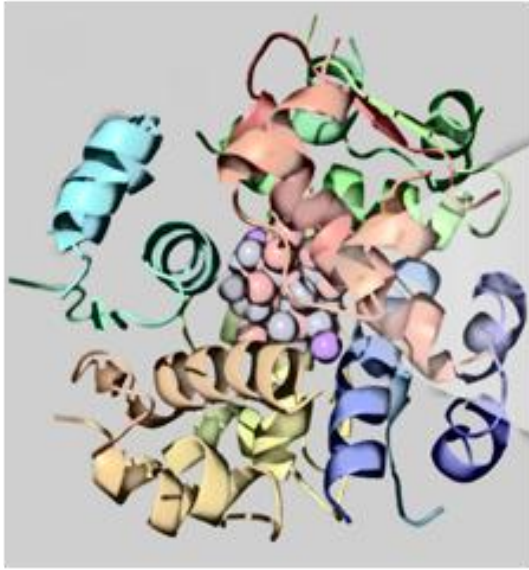
[17]

[20] O. Antonoglou, K. Giannousi, J. Arvanitidis, S. Mourdikoudis, A. Pantazaki, C. Dendrinou-Samara, Elucidation of one step synthesis of PEGylated CuFe bimetallic nanoparticles. Antimicrobial activity of CuFe@PEG vs Cu@PEG, *J. Inorg. Biochem.* 2017, 177:159-170.

[21] K. Giannousi, E. Hatzivassiliou, S. Mourdikoudis, G. Vourlias, A. Pantazaki and C. Dendrinou-Samara, Synthesis and biological evaluation of PEGylated CuO nanoparticles, *J. Inorg. Biochem.* 2016, 164:82-90.

[22] K. Giannousi, M. Menelaou, J. Arvanitidis, M. Angelakeris, A. Pantazaki, C. Dendrinou-Samara, Hetero-nanocomposites of magnetic and antifungal nanoparticles as a platform for magnetomechanical stress induction in *Saccharomyces cerevisiae*, *J. Mater. Chem. B* 2015, 3:5341-5351.

[23] K. Giannousi, G. Sarafidis, S. Mourdikoudis, A. Pantazaki, C. Dendrinou-Samara, Selective Synthesis of Cu_2O and Cu/Cu_2O NPs: Antifungal Activity to Yeast *Saccharomyces cerevisiae* and DNA Interaction, *Inorg. Chem.* 2014, 53:9657−9666.

[24] C. Iannuzzi , M. Borriello, M. Portaccio, *et al.* Insights into Insulin Fibril Assembly at Physiological and Acidic pH and Related Amyloid Intrinsic Fluorescence, *Int J Mol Sci.* 2017 28;18(12).

[25] X.J. Ma, Y.J. Zhang, C.M. Zeng, Inhibition of amyloid aggregation of bovine serum albumin by sodium dodecyl sulfate at submicellar concentrations, *Biochemistry (Mosc).* 2018, 83(1):60-68.

[26] E. L. Gelamoa, CHTP. Silvab, H. Imasatoa, M. Tabaka. Interaction of bovine (BSA) and human (HSA) serum albumins with ionic surfactants: spectroscopy and modelling. Protein Structure and Molecular *Enzymology* 2002, 1594(1), 84-99.

[27] E. Mohammadi, M. Aliofkhazraei, M. Hasanpoor & M. Chipara, Hierarchical and Complex ZnO Nanostructures by Microwave-Assisted Synthesis: Morphologies, Growth Mechanism and Classification, *Critical Reviews in Solid State and Materials Sciences* 2018, 43:6, 475-541.

[28] K. Vamvakidis, M. Katsikini, G. Vourlias, M. Angelakeris, C. E. Paloura, C. Dendrinou-Samara, Composition and hydrophilicity control of Mn-doped ferrite ($Mn_xFe_{3-x}O_4$) nanoparticles induced by polyol differentiation, *Dalton Trans* 2015, 44, 5396–5406.

[29] K. J. Rao, B. Vaidhyanathan, M. Ganguli, P. A. Ramakrishnan, Synthesis of inorganic solids using microwaves, *Chem Mater.* 1999, 11, 882–895.

[30] K. Vamvakidis, M. Katsikini, G. Vourlias *et al.* Composition and hydrophilicity control of Mn-doped ferrite ($Mn_xFe_{3-x}O_4$) nanoparticles induced by polyol differentiation, *Dalton Trans.*, 2015, 44, 5396.

[31] O. Antonoglou, K. Giannousi, J. Arvanitidis *et al.* Elucidation of one step synthesis of PEGylated CuFe bimetallic nanoparticles. Antimicrobial activity of CuFe@PEG vs Cu@PEG, *J. Inorg.Biochem.* 2017, 177, 159–170.

[32] Ali Khorsand Zak, Rehana Razali, Abd Majid W.H, Majid Darroudi, Synthesis and characterization of a narrow size distribution of zinc oxide nanoparticles, *International Journal of Nanomedicine* 2011, No. 6, Pages: 1399–1403.

[33] S. Mourdikoudis, T. Altantzis, L.M. Liz-Marzán *et al.* Hydrophilic Pt nanoflowers: synthesis, crystallographic analysis and catalytic performance, *CrystEngComm* 2016, 18, 3422.

[34] J.J. Schneider, R.C. Hoffmann, J. Engstler, A. Klyszcz, E. Erdem, *et al.* Synthesis, Characterization, Defect Chemistry, and FET Properties of Microwave-Derived Nanoscaled Zinc Oxide, *Chem. Mater.* 2010, Vol. 22, No. 7, Pages: 2203–2212.

[35] A. Antosova, Z. Bednarikova, M. Koneracka *et al.* Destroying activity of glycine coated magnetic nanoparticles on lysozyme, α-lactalbumin, insulin and α-crystallin amyloid fibrils, *Journal of Magnetism and Magnetic Materials* 2019, 471, 169–176.

[36] R. Yousefi, B. Taheri, P. Alavi, M. Bagher Shahsavani, Z. Asadi, *et al.* Aspirin-mediated acetylation induces structural alteration and aggregation of bovine pancreatic insulin, *J Biomol Struct Dyn*. 2016, 34(2):362-75.

[37] M. Bhattacharya, N. Jain, S. Mukhopadhyay, Insights into the Mechanism of Aggregation and Fibril Formation from Bovine Serum Albumin, *J. Phys. Chem. B* 2011, 115, 4195–4205.

[38] S. Asthana, Z. Hazarika, P.S. Nayak *et al.* Insulin adsorption onto zinc oxide nanoparticle mediates conformational rearrangement into amyloid-prone structure with enhanced cytotoxic propensity, *Bbagen* 2018, doi:10.1016/j.bbagen.2018.10.004.

[39] S. Sen, S. Konar, A. Pathak *et al.* Effect of Functionalized Magnetic $MnFe_2O_4$ Nanoparticles on Fibrillation of Human Serum Albumin, *J. Phys. Chem. B* 2014, 118, 11667−11676.

[40] N. Akhtar, S.K. Metkar, A. Girigoswami, K. Girigoswami, ZnO nanoflower based sensitive nano-biosensor for amyloid detection, *Materials Science and Engineering C* 2017, 78, 960–968.

[41] K. Girigoswami, S. H. Ku, J. Ryu, C. B. Park, A synthetic amyloid lawn system for high-throughput analysis of amyloid toxicity and drug screening, *Biomaterials* 2008, 29, 2813–2819.

[42] M.T. Mawhinney, T.L. Williams, J.L. Hart *et al.* Elucidation of insulin assembly at acidic and neutral pH: Characterization of low molecular weight oligomers, *Proteins* 2017, 85, 2096–2110.

[43] C. Iannuzzi, M. Borriello, M. Portaccio *et al.* Insights into Insulin Fibril Assembly at Physiological and Acidic pH and Related Amyloid Intrinsic Fluorescence, *Int. J. Mol. Sci.* 2017, 18, 2551.

[44] K.A. Majorek, P.J. Porebski, A. Dayal, M.D. Zimmerman, K. Jablonska, A.J. Stewart, M. Chruszcz, W. Minor, Structural and immunologic characterization of bovine, horse, and rabbit serum albumins, *Mol Immunol.* 2012, 52(3-4):174-82.

[45] F. Karavassili, A. Valmas, S. Fili, C.D. Georgiou, I. Margiolaki, In Quest for Improved Drugs against Diabetes: The Added Value of X-ray Powder Diffraction Methods, *Biomolecules* 2017, 22;7(3). pii: E63.

[46] G. Hosseinzadeh, A. Maghari, S.M.F. Farnia, A.A. Moosavi-Movahedi, Interaction mechanism of insulin with ZnO nanoparticles by replica exchange molecular dynamics simulation, *J Biomol Struct Dyn.* 2018, 36(14):3623-3635.

[47] a) H.M. Berman, J. Westbrook, Z. Feng, G. Gilliland, T.N. Bhat, *et al.* The Protein Data Bank, *Nucleic Acids Res.* 2000, 28235-242.

b) H.M. Berman, K. Henrick, H. Nakamura, Announcing the worldwide Protein Data Bank, *Nature Struct. Mol. Biol.* 2003, 10, 980.

c) F.C. Bernstein, T.F. Koetzle, G.J. Williams, E.E. Meyer, M.D. Brice, *et al.* The Protein Data Bank: a computer-based archival file for macromolecular structures, *J. Mol. Biol.* 1977,112, 535-542.

[48] A. Bujacz, K. Zielinski, B. Sekula, Structural studies of bovine, equine, and leporine serum albumin complexes with naproxen, *Proteins* 2014, 82, 2199-208.

[49] W.L. DeLano, The PyMOL Molecular Graphics System 0.99, DeLano Scientific, San Carlos, CA, USA (2006).

5. Table of Contents

Molecular Docking of Nanostructures into Insulin

100 nm

ZnO Nanoflowers